On the sound field of a circular membrane in free space and an infinite baffle

Tim Mellow[a)]
Nokia UK Ltd., Farnborough, Hants GU14 0NG, United Kingdom

Leo Kärkkäinen
Nokia Research Center, Helsinki, Finland

(Received 26 April 2006; revised 4 July 2006; accepted 18 August 2006)

An enhanced method for calculating the radiation characteristics of a tensioned circular membrane in free space is presented using an analytical solution to the infinite integral in the free-space Green's function in cylindrical coordinates. This enables direct calculation of the surface pressure series coefficients by equating the coefficients of the resulting Bessel series in a set of simultaneous equations. Eliminating both numerical integration and least-squares minimization improves calculation speed and accuracy. An infinite baffle is introduced to provide an indication of what the theoretical limit of the bass performance would be using a very large enclosure. Furthermore, analytical solutions to the pressure field integrals are presented. A force transmission coefficient is introduced, which is the ratio of the total radiation impedance to the motional impedance. The motional, radiation, and diaphragm impedances of the damped membrane are calculated, together with the near- and far-field pressure responses and efficiency. A comparison is made between the on-axis response (without damping) calculated using this method and using a finite element model. It is demonstrated that good correlation between the two calculation methods can be achieved provided the elements are small enough and a sufficiently large model is used at the frequency extremes. © *2006 Acoustical Society of America.* [DOI: 10.1121/1.2354041]

PACS number(s): 43.20.Rz, 43.20.Tb, 43.40.Dx, 43.38.Ja [LLT] Pages: 2460–2477

I. INTRODUCTION

Interest in electrostatic loudspeakers continues due to their superior performance[1] in terms of low distortion and relatively flat frequency response when suitably damped. Recent advances in digital amplifiers enable improvements in efficiency due to the fact that the reactive current drawn by the static capacitance does not produce the losses that occur with an analogue amplifier. If the loudspeaker has no damping or other kinds of resistance, then there are virtually no losses at all. However, damping, in the form of small holes in the electrodes, is usually applied in order to control the vibrational modes of the membrane. Hence it is useful to derive formulas for the motional input impedance of such a loudspeaker, since this enables its efficiency to be calculated.

The most commonly used model for a loudspeaker is the rigid piston, which assumes global loading over the surface. However, this is not necessarily appropriate in the case of a membrane where there is very strong localized coupling with the acoustic load. Because it is so light, most of the moving mass of the membrane is due to the surrounding fluid medium. Also, because it is acoustically transparent, it would be interesting to see how the pressure field might differ from that of a rigid piston which forms an effectively opaque sound source.

Additionally, the analytical solution to the pressure field of a circular membrane provides a useful benchmark for fluid-structure coupled simulation using the finite element modeling (FEM) method. The latter requires the membrane to be simulated in a virtual anechoic chamber filled with air elements. In this study the analytical solution is used as a reference in order to determine how large this space needs to be in order to match the far-field response. In theory, the anechoic space should be at least as large as the near-field or Fraunhofer zone, which is known to extend further from the source at higher frequencies.[2] Without a baffle, the source becomes a dipole, so the near field extends further from the source at low frequencies too, due to the proximity effect, which, in microphone terminology,[3] is sometimes referred to as "bass tip-up."

The electrostatic circular membrane loudspeaker is one of only a few kinds of transducer which can be completely simulated analytically (except turbulent flow effects between the electrodes and other nonlinear effects are not considered here). By contrast, the electrodynamic speaker is notoriously difficult to model rigorously, due to complicated cone geometries and scattering of the rear wave by the magnet and basket structures. Nearly 20 years after it was first published, Streng's method[4,5] for calculating the sound radiation characteristics of a circular stretched membrane in free space is still the best available. The secret to its success is the ingenious use of a trial function for the surface pressure term of the Kirchhoff-Helmholtz boundary integral, which is derived from Bouwkamp's solution[6] to the free space wave equation in oblate spheroidal coordinates. In fact, this is a somewhat special function since it appears to lead to the simplest possible analytical solution, especially regarding the evaluation of the impedances and near-field pressure. Unlike Streng,

[a)]Electronic mail: tim.mellow@nokia.com

though, the current paper presents a Bessel series matching that eliminates the need for numerical integration and least mean square minimization in the solution.

Whereas the sound radiation from a membrane in free space is calculated using the *dipole* part of the Kirchhoff-Helmholtz boundary integral formula[7] together with a power series expression for the surface *pressure*, the sound radiation from a membrane in an infinite baffle is calculated using the *monopole* part of the Kirchhoff-Helmholtz boundary integral formula together with a similar power series expression, but this time for the surface *velocity*.

Hence, the derivation for the latter has some similarities with that of a plane wave passing through a hole in an infinite screen.[6,8–10] The sound scattered from the hole can be considered as that radiated from a resilient disc in an infinite baffle if the (constant) driving pressure over its surface is equivalent to that of the incident wave in the absence of any obstacle. However, unlike the hole or resilient disc, the membrane does not exhibit infinite velocity near its perimeter, due to the fact that it is anchored at its rim. Hence, the solution to the wave equation for the surrounding medium has to be coupled to that of the membrane and solved simultaneously. Suzuki and Tichy[11] solved the coupled equations for a circular plate, but their formulation relied upon numerical integration. In a previous analysis of a membrane by the present authors,[12] numerical integration was avoided, but the least mean squares algorithm was used to solve the coupled equations, which caused some numerical difficulties. In this paper, the deflection trial function is expanded using a Bessel series so that the coefficients can be calculated directly without either least squares minimization or numerical integration.

The parameters chosen for the undamped FEM and analytical responses are the same as those used by Streng[4] for a 250-mm-diam membrane in free space in order to allow direct comparison. Otherwise, analytical characteristics are calculated for a 500-mm-diam membrane with and without damping in order to represent a typical full frequency range commercial design.

II. MEMBRANE IN FREE SPACE

A. Boundary conditions

The equations that follow are written in axisymmetric cylindrical coordinates, with w as the radial ordinate and z as the axial ordinate. The electrostatic driving pressure $\tilde{p}_I$ is used as the input in a wave equation for the membrane. The tilde denotes a harmonically time varying quantity where the factor $e^{i\omega t}$ is suppressed. The membrane deflection $\tilde{\eta}(w)$ (in the z direction) is then used as a parameter to couple it to the surrounding loss-free acoustic medium. Hence the membrane and free space wave equations must be solved simultaneously. The membrane, with radius a, lies in the xy plane as shown in Fig. 1 with its center at the origin and the uniform driving pressure $\tilde{p}_I$ is applied to its surface in the z direction. The pressure field on one side of the xy plane is the symmetrical "negative" of that on the other, so that

$$\tilde{p}(w,z) = -\tilde{p}(w,-z). \tag{1}$$

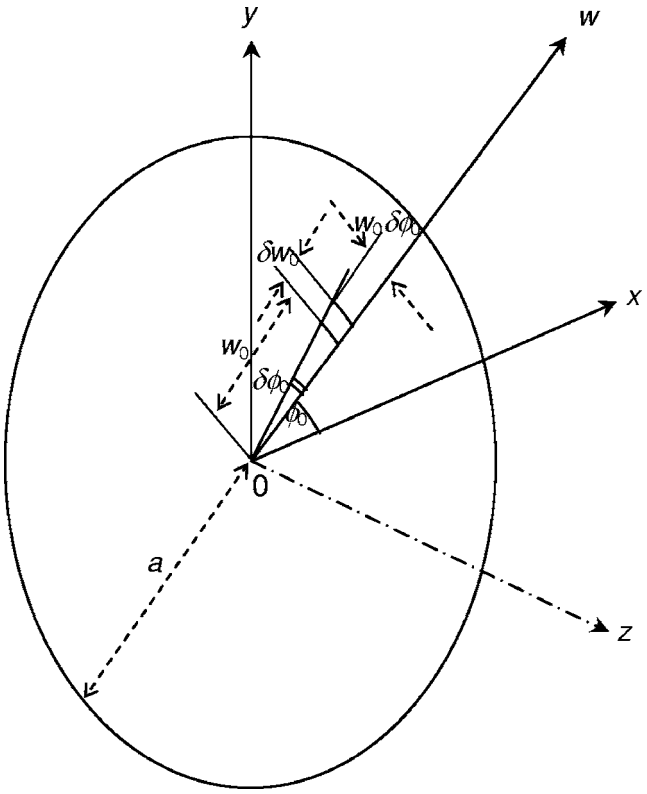

FIG. 1. Geometry of membrane.

Consequently, there is a *Dirichlet* boundary condition in the plane of the membrane where these equal and opposite fields meet, so that

$$\tilde{p}(w,0) = 0, \quad w > a. \tag{2}$$

On the front and rear outer surfaces of the membrane, there is the coupling condition

$$\frac{\partial}{\partial z}\tilde{p}(w,z)|_{z=0\pm} = -ik\rho c\tilde{u}_0(w), \\ = k^2\rho c^2\eta(w), \quad 0 \leqslant w \leqslant a \tag{3}$$

where $\tilde{u}_0(w)$ is the normal particle velocity in the z direction at the surfaces and k is the wave number given by

$$k = \frac{\omega}{c} = \frac{2\pi}{\lambda}, \tag{4}$$

where ω is the angular frequency of excitation, ρ is the density of air or any other surrounding medium, c is the speed of sound in that medium, and λ is the wavelength. Values of 1.18 kg/m^3 and 345 m/s are assumed for ρ and c, respectively. The perimeter of the membrane is fixed, which leads to the following boundary condition:

$$\tilde{\eta}(a) = 0. \tag{5}$$

Streng[4,5] showed that the surface pressure distribution $\tilde{p}_+(w_0)$ for any flat axially symmetric unbaffled source (or sink), based upon Bouwkamp's solution[1] to the free space wave equation in oblate spheroidal coordinates could be written as

$$\tilde{p}_+(w_0) = -\tilde{p}_-(w_0) = \sum_{m=0}^{\infty} \tilde{A}_m \left(1 - \frac{w_0^2}{a^2}\right)^{m+(1/2)}, \tag{6}$$

where $\tilde{A}_m$ are the as yet unknown power series coefficients.

B. Solution to the free space wave equation

1. Rigorous solution

The expression for the pressure field is the same as that given by Eq. (15) (evaluated at $b=a$) in a recent paper on the sound field of disk in a finite circular baffle.[13] The reason why the same formula can be applied to a nonrigid source is that it just describes the sound field due to an arbitrary pressure distribution at the source given by Eq. (6), regardless of the deflection/velocity distribution,

$$\tilde{p}(w,z) = -a\sum_{m=0}^{\infty} \tilde{A}_m \Gamma\left(m+\frac{3}{2}\right) \int_0^{\infty} \left(\frac{2}{\mu a}\right)^{m+(1/2)} J_{m+(3/2)} \times (\mu a) J_0(\mu w) e^{-i\sigma z} d\mu, \tag{7}$$

where

$$\sigma = \begin{cases} \sqrt{k^2-\mu^2}, & 0 \leqslant \mu < k \\ i\sqrt{\mu^2-k^2}, & \mu > k \end{cases} \tag{8}$$

and the power series coefficients $\tilde{A}_m$ are related to normalized dimensionless coefficients τ_m by

$$\tilde{A}_m = \tau_m (m+3/2)\frac{\tilde{p}_I}{2}. \tag{9}$$

Applying the boundary condition of Eq. (3) and truncating the power series limit leads to an expression for the surface particle displacement $\tilde{\eta}(w)$ as follows:

$$\begin{aligned} \tilde{\eta}(w) &= \frac{1}{k^2\rho c^2}\frac{\partial}{\partial z}\tilde{p}(w,z)\big|_{z=0\pm} \\ &= i\frac{a\tilde{p}_I}{2k^2\rho c^2}\sum_{m=0}^{\infty} \tau_m \Gamma\left(m+\frac{5}{2}\right)\int_0^{\infty}\left(\frac{2}{\mu a}\right)^{m+(1/2)} \times J_{m+(3/2)}(\mu a) J_0(\mu w)\sigma d\mu. \end{aligned} \tag{10}$$

The solution[13] to the infinite integral is given by

$$\tilde{\eta}(w) = i\frac{\tilde{p}_I}{2k^2 a\rho c^2}\sum_{m=0}^{M} \tau_m I_m(w,k), \tag{11}$$

where

$$I_m(w,k) = I_{mR}(w,k) + iI_{mI}(w,k), \tag{12}$$

the real part of which is defined by

$$I_{mR}(w,k) = \sqrt{\pi}\sum_{q=0}^{Q}\sum_{r=0}^{R} \frac{(-1)^{q+r}\Gamma(m+5/2)}{(q!)^2 r!\Gamma(r+m+5/2)} \times \frac{\Gamma(q+r+1)}{\Gamma(q+r+5/2)}\left(\frac{ka}{2}\right)^{2(q+r)+3}\left(\frac{w}{a}\right)^{2q}, \tag{13}$$

and the imaginary part is defined by

$$I_{mI}(w,k) = \sqrt{\pi}\sum_{q=0}^{Q}\sum_{r=0}^{R} \frac{(-1)^{q+r+m}\Gamma(m+5/2)}{(q!)^2 r!\Gamma(r-m-1/2)} \times \frac{\Gamma(q+r-m-1/2)}{\Gamma(q+r-m+1)}\left(\frac{ka}{2}\right)^{2(q+r-m)}\left(\frac{w}{a}\right)^{2q}. \tag{14}$$

Let

$$\left(\frac{w}{a}\right)^{2q} = \sum_{n=1}^{\infty} a_n J_0(\alpha_n w/a), \tag{15}$$

where α_n is the nth zero of $J_0(\alpha_n)$ [i.e., nth solution of $J_0(\alpha_n)=0$]. Multiplying through by the normalizing function $J_0(\alpha_n w/a)$ and integrating over w while applying the property of orthogonality leads to

$$\begin{aligned} a_n &= \frac{\int_0^a (w/a)^{2q} J_0(\alpha_k w/a) w dw}{\int_0^a J_0(\alpha_n w/a) J_0(\alpha_k w/a) w dw} \\ &= \frac{{}_1F_2(q+1);1,\ q+2;-\alpha_n^2/4)}{(q+1)J_1^2(\alpha_n)}, \end{aligned} \tag{16}$$

where the following identities[14,15] have been used:

$$\int_0^a J_0(\alpha_n w/a) J_0(\alpha_k w/a) w dw = \begin{cases} a^2 J_1^2(\alpha_n)/2, & \alpha_k = \alpha_n \\ 0, & \alpha_k \neq \alpha_n, \end{cases} \tag{17}$$

$$\int_0^a \left(\frac{w}{a}\right)^{2q} J_0(\alpha_k w/a) w dw = \frac{a^2\,{}_1F_2(q+1;1,q+2;-\alpha_k^2/4)}{2(q+1)}. \tag{18}$$

Hence

$$\tilde{\eta}(w) = i\frac{\tilde{p}_I}{2k^2 a\rho c^2}\sum_{m=0}^{M}\tau_m \sum_{q=0}^{Q}({}_m\mathbf{B}_q(ka) + i\,{}_m\mathbf{S}_q(ka)) \times \sum_{n=1}^{N}\frac{{}_1F_2(q+1;1,q+2;-\alpha_n^2/4)}{(q+1)J_1^2(\alpha_n)} J_0(\alpha_n w/a), \tag{19}$$

where $\mathbf{S}$ and $\mathbf{B}$ are dipole cylindrical wave functions. $\mathbf{S}$ has been named the Streng function[13] as defined by

$${}_m\mathbf{S}_q(kb) = \sqrt{\pi}\sum_{r=0}^{R}\frac{(-1)^{q+r+m}(ka/2)^{2(q+r-m)}}{r!(q!)^2(m+5/2)_{r-2m-3}(q+r-m-1/2)_{3/2}} \tag{20}$$

and $\mathbf{B}$ has been named the Bouwkamp function[13] as defined by

$${}_m\mathbf{B}_q(kb) = \sqrt{\pi}\sum_{r=0}^{R}\frac{(-1)^{q+r}(ka/2)^{2(q+r)+3}}{r!(q!)^2(m+5/2)_r(q+r+1)_{3/2}}. \tag{21}$$

where $(x)_n$ is the Pochhammer symbol.

2. High frequency approximation

At high frequencies, the following approximation can be used:

$$I_m(w,k) \approx a^2\Gamma\left(m+\frac{5}{2}\right)\int_0^\infty \left(\frac{2}{a\mu}\right)^{m+(1/2)} J_{m+(3/2)} \times (a\mu)J_0(w\mu)kd\mu, \tag{22}$$

the solution[16] to which is given by

$$I_m(w,k) \approx ka\left(m+\frac{3}{2}\right)\left(1-\frac{w^2}{a^2}\right)^{m+(1/2)}. \tag{23}$$

Let

$$\left(1-\frac{w^2}{a^2}\right)^{m+(1/2)} = \sum_{n=1}^{\infty} a_n J_0(\alpha_n w/a), \tag{24}$$

so that multiplying through by the normalizing function $J_0(\alpha_k w/a)$ and integrating over w while applying the property of orthogonality leads to

$$a_n = \frac{\int_0^a (1-(w/a)^2)^{m+(1/2)} J_0(\alpha_k w/a) w dw}{\int_0^a J_0(\alpha_n w/a)J_0(\alpha_k w/a) w dw} = \Gamma\left(m+\frac{3}{2}\right)\left(\frac{2}{\alpha_n}\right)^{m+(3/2)} \frac{J_{m+(3/2)}(\alpha_n)}{J_1^2(\alpha_n)}, \tag{25}$$

where Sonine's integral[14] has been used as follows:

$$\int_0^a \left(1-\frac{w_0^2}{a^2}\right)^{m+(1/2)} J_0(\alpha_n w_0/a) w_0 dw_0 = \frac{a^2}{2}\Gamma\left(m+\frac{3}{2}\right)\left(\frac{2}{\alpha_n}\right)^{m+(3/2)} J_{m+(3/2)}(\alpha_n) \tag{26}$$

together with Eq. (17). Hence

$$\tilde{\eta}(w) \approx \frac{i\tilde{p}_I}{2k\rho c^2}\sum_{m=0}^{\infty}\tau_m\Gamma\left(m+\frac{5}{2}\right)\sum_{n=1}^{\infty}\left(\frac{2}{\alpha_n}\right)^{m+(3/2)} \times \frac{J_{m+(3/2)}(\alpha_n)}{J_1^2(\alpha_n)} J_0(\alpha_n w/a). \tag{27}$$

C. Membrane wave equation

The loudspeaker configuration is shown in Fig. 2, with stationary electrodes on either side of the membrane, each at a distance d from it. The steady state wave equation for the membrane deflection $\tilde{\eta}(w)$ can be written with the inherent membrane forces on the left and the external forces on the right:

$$(T\nabla^2 - i\omega z_s - \omega^2\rho_D h)\tilde{\eta}(w) = \tilde{p}_+(w) - \tilde{p}_-(w) - \tilde{p}_I, \tag{28}$$

where

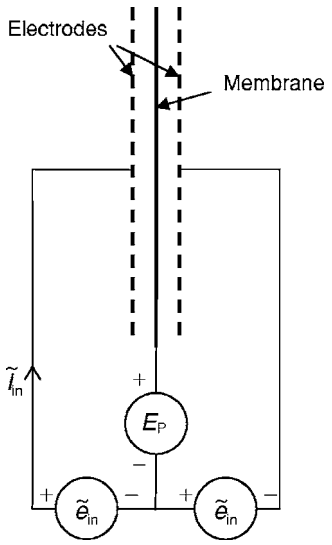

FIG. 2. Electrostatic loudspeaker configuration.

$$\nabla^2 = \frac{\partial^2}{\partial w^2} + \frac{1}{w}\frac{\partial}{\partial w}, \tag{29}$$

where $\tilde{p}_+(w)$ and $\tilde{p}_-(w)$ are the front and rear pressure distributions, respectively, due to the surrounding acoustic medium, T is the tension (which is evenly distributed throughout the membrane), ρ_D is the density of the membrane material, h is its thickness, S is its surface area (given by $S=\pi a^2$), and z_s is an arbitrary specific acoustic impedance which is defined by

$$z_S = R_S + ikcM_S - \frac{C_{\mathrm{ED}}}{ikcS}\left(\frac{E_P}{d}\right)^2, \tag{30}$$

where R_S and M_S are the distributed resistance and mass, respectively, of the perforations in the electrodes on either side of the membrane, which are usually designed to damp its vibration modes[17,18]. For the purpose of this analysis, it is assumed that the mass is negligible and that the resistance is linear and will not vary with frequency. The remaining term is the "negative impedance"[1] that results from the increase in electrostatic attraction toward each electrode as the membrane approaches it. The capacitance C_{ED} between the electrodes is given by

$$C_{\mathrm{ED}} = \varepsilon_0 S/d, \tag{31}$$

where ε_0 is the permittivity of free space. Due to the push-pull arrangement, it is assumed that the change in capacitance on each side of the membrane, as it is displaced, will tend to balance out. Hence the electrostatic forces will hardly vary, providing there is enough tension. The total driving force $\tilde{F}_I$ is related to the driving pressure $\tilde{p}_I$ and input voltage $\tilde{e}_{\mathrm{in}}$ by

$$\tilde{F}_I = S\tilde{p}_I = 2C_{\mathrm{ED}}\frac{E_P}{d}\tilde{e}_{\mathrm{in}}, \tag{32}$$

where E_P is the membrane polarizing voltage and d is the membrane to electrode spacing. Whilst applying Eq. (1) to the rear pressure term, Eq. (28) can be written in the "Helm-

holtz" form using the modified diaphragm wave number k'_D as follows:

$$(\nabla^2 + k'^2_D)\,\tilde{\eta} = \frac{1}{T}(2\tilde{p}_+(w) - \tilde{p}_I), \tag{33}$$

where

$$k'_D(k) = k_D(k)\sqrt{1 - i\frac{z_S}{k_D(k)\sqrt{\rho_D h T}}}, \tag{34}$$

$$k_D(k) = \omega/c_D = kc/c_D, \tag{35}$$

and

$$c_D = \sqrt{\frac{T}{\rho_D h}}, \tag{36}$$

where c_D is the speed of sound in the membrane.

D. Solution of the dynamic membrane wave equation

The solution to membrane wave equation, Eq. (33), subject to the edge constraint of Eq. (5), is essentially a two-dimensional counterpart to the Kirchhoff-Helmholtz volume integral as follows:

$$\tilde{\eta}(w) = \frac{1}{T}\int_0^{2\pi}\int_0^a (2\tilde{p}_+(w_0) - \tilde{p}_I)G(w|w_0)w_0 dw_0 d\phi_0. \tag{37}$$

The Green's function[7] for the membrane can be written using the modified wave number k'_D and suppressing the axial term in ϕ and ϕ_0 as follows:

$$G(w|w_0) = \frac{1}{\pi}\sum_{n=1}^{\infty}\frac{J_0(\alpha_n w/a)J_0(\alpha_n w_0/a)}{J_1^2(\alpha_n)(\alpha_n^2 - k'^2_D a^2)}, \quad 0 \leqslant w \leqslant a, \tag{38}$$

where α_n is the nth zero of $J_0(k'_D a)$ such that $J_0(k'_D a)=0$ when $k'_D a = \alpha_n$. Inserting Eqs. (6), (9), and (38) in Eq. (37) and integrating over the surface of the membrane and baffle yields

$$\tilde{\eta}(w) = -\frac{a^2}{T}\tilde{p}_I\sum_{n=1}^{\infty}\frac{J_0(\alpha_n w/a)}{J_1(\alpha_n)(\alpha_n^2 - k'^2_D a^2)}\left(\frac{2}{\alpha_n} - \sum_{m=0}^{\infty}\tau_m\Gamma\left(m+\frac{5}{2}\right)\times\left(\frac{2}{\alpha_n}\right)^{m+(3/2)}\frac{J_{m+(3/2)}(\alpha_n)}{J_1(\alpha_n)}\right), \tag{39}$$

where the following identity[14] has been used:

$$\int_0^a J_0(\alpha_k w_0/a)w_0 dw_0 = a^2 J_1(\alpha_k)/\alpha_k, \tag{40}$$

together with Eq. (26).

E. Final set of simultaneous equations for the power series coefficients

1. Rigorous solution

Equating the right-hand sides of Eqs. (19) and (39) and then equating the coefficients of $J_0(\alpha_n w/a)$, yields the following set of $M+1$ simultaneous equations in τ_m:

$$\sum_{m=0}^{M} {}_m\Psi_n(k'_D a, ka)\tau_m = 1, \quad n = 1,2,\ldots,M+1, \tag{41}$$

where

$${}_m\Psi_n(k'_D a, ka) = \frac{\alpha_n}{2J_1(\alpha_n)}\left\{\Gamma\left(m+\frac{5}{2}\right)\left(\frac{2}{\alpha_n}\right)^{m+(3/2)} \times J_{m+(3/2)}(\alpha_n) - \frac{\alpha_n^2 - k'^2_D a^2}{\alpha^2(ka)} \times\sum_{q=0}^{Q}({}_m\mathbf{S}_q(ka) + i\,{}_m\mathbf{B}_q(ka)) \times \frac{{}_1F_2(q+1;1,q+2;-\alpha_n^2/4)}{q+1}\right\} \tag{42}$$

and

$$\alpha(ka) = a\omega\sqrt{\frac{2a\rho}{T}} = ka\sqrt{\frac{2a\gamma P_0}{T}}, \tag{43}$$

where the infinite series have been truncated to orders M, Q, and R. $\mathbf{S}$ and $\mathbf{B}$ are dipole cylindrical wave functions defined in Eqs. (20) and (21), respectively. The dimensionless parameter α is the fluid-loading factor, where P_0 is the static pressure defined by $P_0 = \rho c^2/\gamma$ and γ is the adiabatic index. The calculations were performed using, in the case of the damped membrane, 50 digit precision with $M = 10 + ka$ and $Q = R = 2M$. In the case of the undamped membrane, 100 digit precision was used with $M = 10 + 5ka$ and again $Q = R = 2M$.

2. High frequency approximation

For large values of ka, the following high-frequency approximation can be obtained by equating the right-hand sides of Eqs. (27) and (39) and then equating the coefficients of $J_0(\alpha_{0n} w/a)$ so that

$${}_m\Psi_n(k'_D a, ka) \approx \Gamma\left(m+\frac{5}{2}\right)\left(\frac{2}{\alpha_n}\right)^{m+(1/2)}\frac{J_{(m+3/2)}(\alpha_n)}{J_1(\alpha_n)} \times\left\{1 - \frac{ika(\alpha_n^2 - k'^2_D a^2)}{\alpha^2(ka)}\right\}. \tag{44}$$

F. Impedance and efficiency

1. Input impedance

The total volume velocity $\tilde{U}_0$ produced by the membrane is equal to the integral of its velocity $\tilde{u}_0(w)(=i\omega\tilde{\eta}(w))$ from Eq. (10) over its surface as follows:

$$\tilde{U}_0 = ikc\int_0^{2\pi}\int_0^a \tilde{\eta}(w)w\,dw\,d\phi$$
$$= \frac{a\tilde{F}_I}{2k\rho c}\sum_{m=0}^{M}\tau_m\Gamma\left(m+\frac{5}{2}\right)\int_0^\infty\left(\frac{2}{a\mu}\right)^{m+3/2}$$
$$\times J_{m+3/2}(a\mu)J_1(a\mu)\sqrt{k^2-\mu^2}\,d\mu, \tag{45}$$

where the identity of Eq. (40) has again been used. Finally, after solving the infinite integral[15]

$$\tilde{U}_0 = \frac{\tilde{F}_I}{2\rho c}\sum_{m=0}^{M}\tau_m\left\{1-{}_2F_3\left(\frac{m}{2}+\frac{3}{4},\frac{m}{2}+\frac{5}{4};\frac{3}{2},m+\frac{3}{2},m+\frac{5}{2};-k^2a^2\right)\right.$$
$$\left.-i\frac{{}_2F_3\left(\frac{m}{2}+\frac{1}{4},\frac{m}{2}+\frac{3}{4};\frac{1}{2},m+1,m+2;-k^2a^2\right)}{ka(m+1/2)_{1/2}(m+5/2)_{-1/2}}\right\}. \tag{46}$$

The mechanical motional impedance z_{mi} is simply the ratio of the applied force $\tilde{F}_I$ to the average membrane velocity. It can also be expressed in terms of the volume velocity

$$z_{\mathrm{mi}} = \frac{\tilde{F}_I}{\tilde{u}_0} = \frac{S\tilde{F}_I}{\tilde{U}_0} = 2S\rho cZ_I, \tag{47}$$

where the normalized motional input impedance Z_I is given by

$$Z_I = \frac{\tilde{F}_I}{2\rho c\tilde{U}_0}. \tag{48}$$

Then z_E is the electrical input impedance, which is given by

$$z_E = \frac{z_{\mathrm{ES}}z_{\mathrm{EM}}}{z_{\mathrm{ES}}+z_{\mathrm{EM}}}, \tag{49}$$

where z_{ES} is the *static* electrical impedance given by

$$z_{\mathrm{ES}} = \frac{1}{i\omega C_{\mathrm{ED}}} = \frac{d}{i\omega\varepsilon_0 S} \tag{50}$$

and z_{EM} is the *motional* electrical impedance given by

$$z_{\mathrm{EM}} = \frac{z_{\mathrm{mi}}}{2(C_{\mathrm{ED}}E_P/d)^2}. \tag{51}$$

The input impedance for a damped membrane is shown in Fig. 3. Since the static impedance dominates, the motional impedance is plotted separately in Fig. 4.

2. Radiation impedance

The total radiation force $\tilde{F}_R$ acting upon the membrane can be found by integrating the surface pressure from Eq. (6) over its surface as follows:

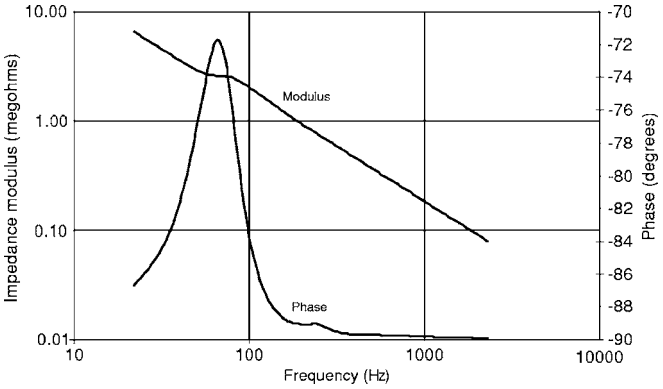

FIG. 3. Electrical input impedance of push-pull electrostatic loudspeaker in free space where a=250 mm, h=12 μm, T=700 N/m, ρ_D=1400 kg/m^3, E_P=3000 V, d=2 mm, r=1 m and R_S=100 Ns/m^3.

$$\tilde{F}_R = -\int_0^{2\pi}\int_0^a \tilde{p}_+(w_0)w_0\,dw_0\,d\phi_0 = -\frac{\tilde{F}_I}{2}\sum_{m=0}^{M}\tau_m. \tag{52}$$

Let a membrane force transmission coefficient ζ be defined by

$$\zeta = -2\tilde{F}_R/\tilde{F}_I \tag{53}$$

or simply the ratio of the total radiation impedance (on both sides) to the motional impedance. Then from Eq. (52)

$$\zeta = \sum_{m=0}^{M}\tau_m. \tag{54}$$

The acoustic radiation impedance z_{ar} is then given by

$$z_{\mathrm{ar}} = \frac{\tilde{F}_R}{S\tilde{U}_0} = \frac{\rho c}{S}(R_R+iX_R), \tag{55}$$

where R_R is the normalized radiation *resistance* given by $R_R=\Re(\zeta Z_I)$ and X_R is the normalized radiation *reactance* given by $X_R=\Im(\zeta Z_I)$. This result is plotted in Fig. 5 together with the radiation impedance of a rigid disk in free space for comparison.

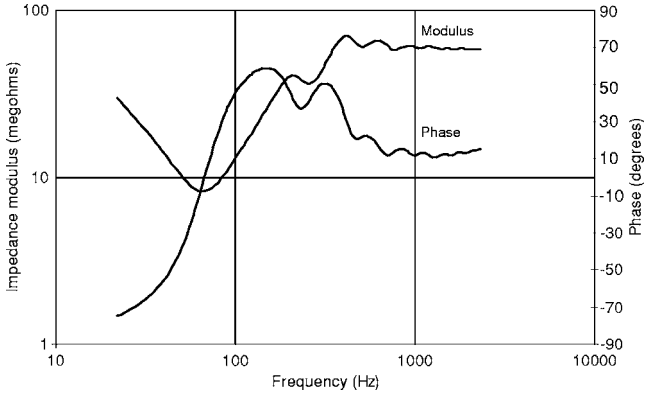

FIG. 4. Motional part of electrical impedance in free space with the same parameters as in Fig. 3.

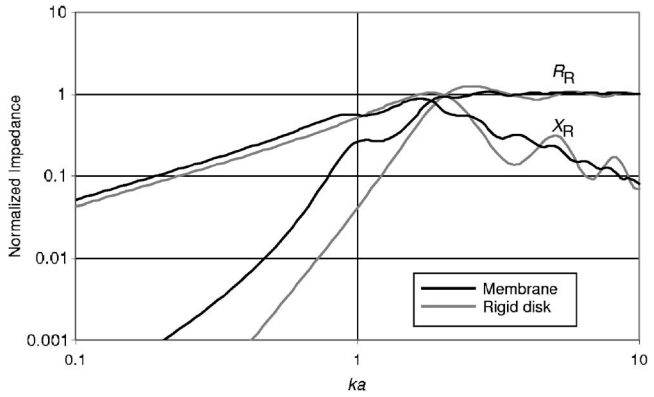

FIG. 5. Normalized radiation impedance in free space with same parameters as in Fig. 3 and radiation impedance of a rigid disk in free space.

3. Efficiency

Now it is easy to calculate the efficiency which is simply equal to $100^{*}R_R/R_I$ and is shown in Fig. 10 along with the far-field on-axis pressure response and peak displacement.

4. Diaphragm impedance

The mechanical diaphragm impedance z_{md} is the difference between the input impedance and the radiation impedance on both sides where

$$z_{\mathrm{md}} = \frac{\tilde{F}_I - 2\tilde{F}_R}{\tilde{u}_0} = \frac{S(\tilde{F}_I - 2\tilde{F}_R)}{\tilde{U}_0} = 2S\rho c(R_D + iX_D), \tag{56}$$

where R_D is the normalized diaphragm *resistance* given by $R_D=\Re(Z_I(1-\zeta))$ and X_D is the normalized membrane *reactance* given by $X_D=\Im(Z_I(1-\zeta))$. This result is plotted in Fig. 6. The various impedances are shown on an equivalent electrical circuit in Fig. 7.

G. Near-field pressure response

1. Near-field pressure as an integral expression

After truncating the summation limit, Eq. (7) can be separated into finite and infinite integrals as follows:

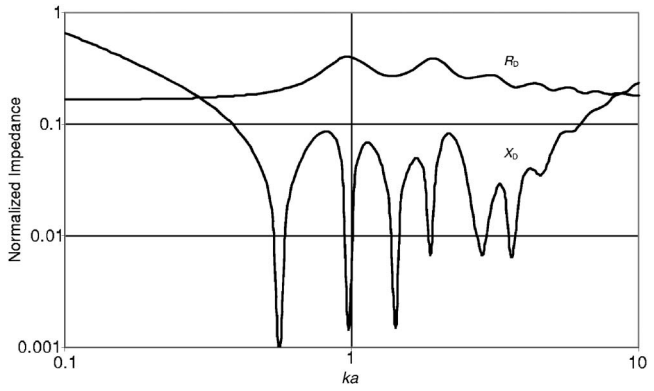

FIG. 6. Normalized diaphragm impedance in free space with the same parameters as in Fig. 3.

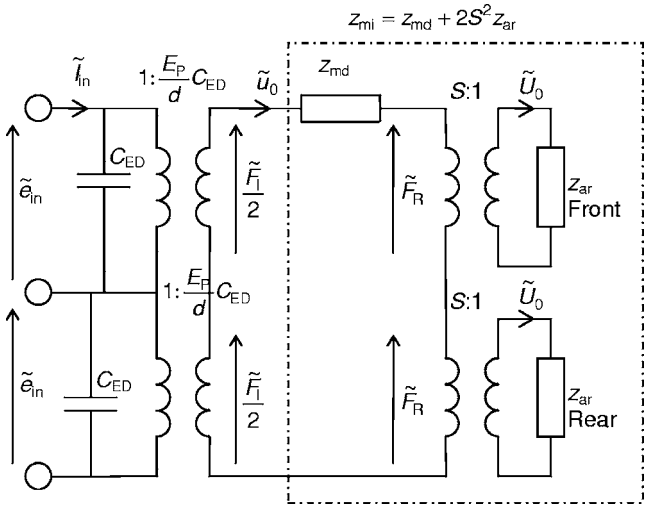

FIG. 7. Equivalent electrical circuit.

$$\tilde{p}(w,z) = -\frac{\tilde{p}_I}{2}\sum_{m=0}^{M}\tau_m\Gamma\left(m+\frac{5}{2}\right)(I_{\mathrm{Fin}}(m,w,z) + I_{\mathrm{Inf}}(m,w,z)), \tag{57}$$

where

$$I_{\mathrm{Fin}}(m,w,z) = a\int_0^k\left(\frac{2}{a\mu}\right)^{m+(1/2)}J_{m+(3/2)}(a\mu) \times J_0(w\mu)e^{-iz\sqrt{k^2-\mu^2}}d\mu \tag{58}$$

and

$$I_{\mathrm{Inf}}(m,w,z) = a\int_k^\infty\left(\frac{2}{a\mu}\right)^{m+(1/2)}J_{m+(3/2)}(a\mu) \times J_0(w\mu)e^{-z\sqrt{\mu^2-k^2}}d\mu, \tag{59}$$

2. Solution of the finite integral

Substituting $\mu=k\sqrt{1-t^2}$ in Eq. (58) in order to simplify the exponent yields

$$I_{\mathrm{Fin}}(m,w,z) = 2\left(\frac{2}{ka}\right)^{m-(1/2)} \times\int_0^1\frac{J_{m+(3/2)}(ka\sqrt{1-t^2})J_0(kw\sqrt{1-t^2})}{(1-t^2)^{(m/2)+(3/4)}}e^{-ikzt}tdt. \tag{60}$$

The Bessel functions in Eq. (60) can then be expanded using the following Lommel expansion:[19]

$$\frac{J_n(ka\sqrt{1-t^2})}{(1-t^2)^{n/2}} = \sum_{m=0}^{\infty}\left(\frac{ka}{2}\right)^m\frac{t^{2m}}{m!}J_{n+m}(ka), \tag{61}$$

which leads to

$$I_{\mathrm{Fin}}(m,w,z) = 2\sum_{p=0}^{\infty}\sum_{q=0}^{\infty}\left(\frac{ka}{2}\right)^{p-m+(1/2)}\left(\frac{kw}{2}\right)^{q} \times \frac{J_{p+m+(3/2)}(ka)J_q(kw)}{p!q!}\int_0^1 e^{-ikzt}t^{2(p+q)+1}dt. \tag{62}$$

The integral in Eq. (62) can be solved using the identity[14]

$$\int_0^1 e^{-ikzt}t^{2(p+q)+1}dt = \frac{\gamma(2p+2q+2,ikz)}{(ikz)^{2(p+q)+2}}, \tag{63}$$

where γ is the incomplete gamma function. Inserting Eq. (63) in Eq. (62) and truncating the summation limits gives the final solution to Eq. (60) as follows:

$$I_{\mathrm{Fin}}(m,w,z) = 2\sum_{p=0}^{P}\sum_{q=0}^{Q}\frac{1}{p!q!(ikz)^{2(p+q+1)}}\left(\frac{ka}{2}\right)^{p-m+(1/2)} \times\left(\frac{kw}{2}\right)^{q}J_{p+m+(3/2)}(ka)J_q(kw) \times\gamma(2p+2q+2,ikz). \tag{64}$$

3. Solution of the infinite integral

a. Expansion of the Bessel functions. Substituting $\mu = k\sqrt{t^2+1}$ in Eq. (59) in order to simplify the exponent yields

$$I_{\mathrm{Inf}}(m,w,z) = 2\left(\frac{2}{ka}\right)^{m-(1/2)}\int_0^{\infty}\frac{J_{m+(3/2)}(ka\sqrt{t^2+1})}{(t^2+1)^{(m/2)+(3/4)}} \times J_0(kw\sqrt{t^2+1})e^{-kzt}tdt. \tag{65}$$

The Bessel functions in Eq. (65) can expanded in two possible ways. The first is the Lommel expansion[19] as follows:

$$\frac{J_n(ka\sqrt{t^2+1})}{(t^2+1)^{n/2}} = \sum_{m=0}^{\infty}(-1)^m\left(\frac{ka}{2}\right)^m\frac{t^{2m}}{m!}J_{m+n}(ka), \tag{66}$$

and the second is Gegenbauer's summation theorem[14]

$$\frac{J_n(ka\sqrt{t^2+1})}{(t^2+1)^{n/2}} = \Gamma(n)\left(\frac{2}{kat}\right)^n\sum_{m=0}^{\infty}(m+n)J_{m+n}(kat) \times J_{m+n}(ka)C_m^n(0), \tag{67}$$

where C_m^n is the Gegenbauer[14] polynomial given by

$$C_m^n(0) = \begin{cases} 1, & m=n=0 \\ \dfrac{\cos(m\pi/2)\Gamma(n+m/2)}{(m/2)!\Gamma(n)}, & m\neq 0 \text{ or } n\neq 0, \end{cases} \tag{68}$$

where n is a positive real integer. Inserting Eq. (68) in Eq. (67) and noting that, due to the cosine term, all odd terms of the Gegenbauer polynomial are zero, yields

$$\frac{J_n(ka\sqrt{t^2+1})}{(t^2+1)^{n/2}} = \begin{cases} 2\displaystyle\sum_{m=0}^{\infty}\frac{(-1)^m}{1+\delta_{0m}}J_{2m}(ka)J_{2m}(kat), & n=0 \\ \left(\dfrac{2}{kat}\right)^n\displaystyle\sum_{m=0}^{\infty}\frac{(-1)^m}{m!}(2m+n)\Gamma(m+n)\times J_{2m+n}(ka)J_{2m+n}(kat), & n\neq 0, \end{cases} \tag{69}$$

where δ_{0m} is the Kronecker delta function. If both Bessel functions were to be expanded (in a procedure similar to that of Williams[20]) using the Lommel expansion of Eq. (66), together with the following identities[14]

$$\int_0^{\infty} e^{-kzt}t^{2(p+q)+1}dt = \frac{\Gamma(2p+2q+2)}{(kz)^{2(p+q)+2}}, \tag{70}$$

$$\gamma(2p+2q+2,ikz) - \Gamma(2p+2q+2) = -\Gamma(2p+2q+2,ikz), \tag{71}$$

the resulting solution

$$I_{\mathrm{Fin}} + I_{\mathrm{Inf}} = 2\sum_{p=0}^{P}\sum_{q=0}^{Q}\frac{1}{p!q!(ikz)^{2(p+q+1)}}\left(\frac{ka}{2}\right)^{p-m+(1/2)}\left(\frac{kw}{2}\right)^{q} \times J_{p+m+(3/2)}(ka)J_q(kw)\Gamma(2p+2q+2,ikz) \tag{72}$$

would only converge for $z^2 \geqslant a^2+w^2$ and would therefore be of limited value. On the other hand, expanding both Bessel functions using the summation theorem leads to an integral of the form

$$\int_0^{\infty} J_{2p+m+(3/2)}(kat)J_{2q}(kwt)e^{-kzt}t^{-1}dt, \tag{73}$$

which can be solved, but the solution is in the form of an expansion and is therefore slow to compute. Hence, the following solution uses the Lommel expansion for one Bessel function and the summation theorem for the other and then exchanges them so that convergent solutions are obtained, in turn, for $0<w^2+z^2\leqslant a^2$ and $w^2+z^2\geqslant a^2$ (providing $z>0$).

b. Solution when the distance from the center of the membrane to the observation point is greater than the membrane's radius Expanding $J_{m+(3/2)}(ka\sqrt{t^2+1})$ in Eq. (65) with Eq. (66) and $J_0(kw\sqrt{t^2+1})$ with Eq. (69) yields

$$I_{\mathrm{Inf}}(m,w,z) = 4\sum_{p=0}^{\infty}\sum_{q=0}^{\infty}\frac{(-1)^{p+q}}{p!(1+\delta_{0q})}\left(\frac{ka}{2}\right)^{p-m+(1/2)} \times J_{p+m+(3/2)} \times (ka)J_{2q}(kw)\int_0^{\infty} e^{-kzt}J_{2q}(kwt)t^{2p+1}dt. \quad (74)$$

The integral in Eq. (74) can be solved using the following identity:[14]

$$\int_0^{\infty} e^{-kzt}J_{2q}(kwt)t^{2p+1}dt = \frac{\Gamma(2p+2q+2)}{(k^2z^2+k^2w^2)^{p+1}} \times P_{2p+1}^{-2q}\left(\frac{z}{\sqrt{z^2+w^2}}\right), \quad (75)$$

so that, after truncating the summation limits, the final solution is given by

$$I_{\mathrm{Inf}}(m,w,z) = 4\sum_{p=0}^{P}\sum_{q=0}^{Q}\frac{(-1)^{p+q}\Gamma(2p+2q+2)}{(1+\delta_{0q})p!(k^2z^2+k^2w^2)^{p+1}} \times \left(\frac{ka}{2}\right)^{p-m+(1/2)} J_{p+m+(3/2)}(ka)J_{2q}(kw) \times P_{2p+1}^{-2q}\left(\frac{z}{\sqrt{z^2+w^2}}\right). \quad (76)$$

This expression converges for $w^2+z^2 \geqslant a^2$ and can therefore be used in that region, providing $z>0$.

c. Solution when the distance from the center of the membrane to the observation point is less than the membrane's radius Expanding $J_{m+(3/2)}(ka\sqrt{t^2+1})$ in Eq. (65) with Eq. (69) and $J_0(kw\sqrt{t^2+1})$) with Eq. (66) yields

$$I_{\mathrm{Inf}}(m,w,z) = 2\left(\frac{2}{ka}\right)^{2m+1}\sum_{p=0}^{\infty}\sum_{q=0}^{\infty}\frac{(-1)^{p+q}\Gamma(p+m+3/2)}{p!q!} \times (2p+m+3/2)\left(\frac{kw}{2}\right)^{q} J_{2p+m+(3/2)}(ka) \times J_q(kw)\int_0^{\infty} e^{-kzt}J_{2p+m+(3/2)}(kat)t^{2q-m-(1/2)}dt. \quad (77)$$

The integral in Eq. (77) can be solved using the identity of Eq. (75) so that, after truncating the summation limits, the final solution is given by

$$I_{\mathrm{Inf}}(m,w,z) = 2\left(\frac{2}{ka}\right)^{2m+1}\sum_{p=0}^{P}\sum_{q=0}^{Q}\frac{(-1)^{p+q}(2p+m+3/2)}{q!(k^2z^2+k^2a^2)^{q-(m/2)+(1/4)}} \times (p+1)_{m+(1/2)}\Gamma(2p+2q+2)\left(\frac{kw}{2}\right)^{q} \times J_{2p+m+(3/2)}(ka)J_q(kw)P_{2q-m-(1/2)}^{-2p-m-(3/2)}\left(\frac{z}{\sqrt{z^2+a^2}}\right). \quad (78)$$

This expression converges for $w^2<a^2+z^2$ and can therefore be used in the region $0<w^2+z^2<a^2$, providing $z>0$. The normalized near-field pressure response of the membrane is shown in Fig. 8 for various values of ka. The calculations were performed using 50 digit precision with $M=P=50$ and $Q=100$.

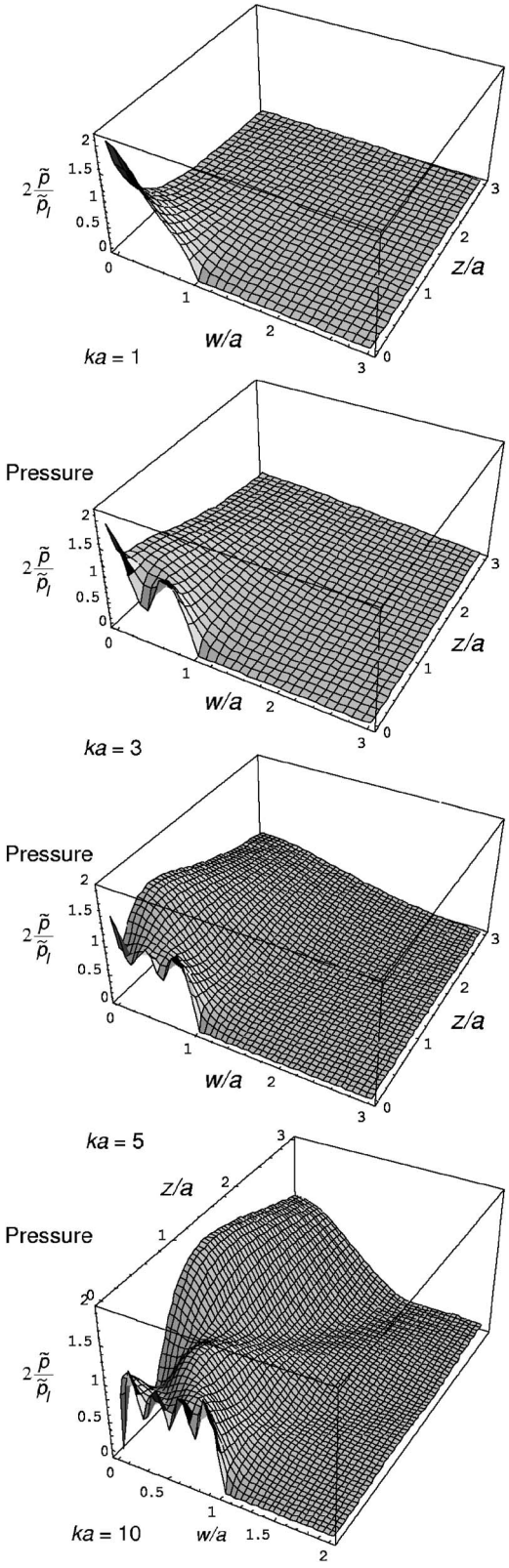

FIG. 8. Near-field pressure response in free space with the same parameters as in Fig. 3.

H. Far-field pressure response

The far-field pressure is derived using the same procedure as shown in Part K of Sec. II of a recent paper [13] to give

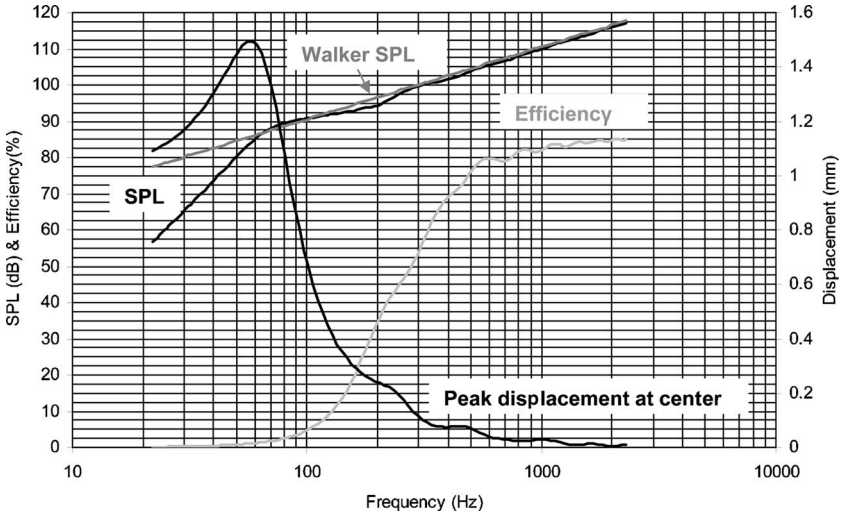

FIG. 9. On-axis pressure response of push-pull electrostatic loudspeaker in free space where $a=250$ mm, $h=12$ μm, $T=700$ N/m, $\rho_D=1400$ kg/m^3, $e_{\text{in}}=2000$ V$_{\text{rms}}$, $E_P=3000$ V, $d=2$ mm, $r=1$ m, and $R_S=100$ Ns/m^3.

$$\tilde{p}(r,\theta) = -i\frac{a\tilde{p}_I}{4r}e^{-ikr}D(\theta) = -i\frac{E_P}{d}C_{\text{ED}}\frac{a\tilde{e}_{\text{in}}}{2rS}e^{-ikr}D(\theta), \quad (79)$$

where the directivity function $D(\theta)$ is given by

$$D(\theta) = ka\cos\theta\sum_{m=0}^{M}\tau_m\Gamma\left(m+\frac{5}{2}\right)\left(\frac{2}{ka\sin\theta}\right)^{m+(3/2)} \times J_{m+3/2}(ka\sin\theta), \quad (80)$$

which, for $\theta=0$ (i.e., on-axis), simplifies to

$$D(0) = ka\sum_{m=0}^{M}\tau_m = ka\zeta, \quad (81)$$

using ζ from Eq. (54). (The on-axis response of a resilient disk in free space is given by setting $\zeta=1$.) The on-axis pressure then simplifies to

$$\tilde{p}(r,0) = -i\frac{ka^2}{4r}\tilde{p}_I e^{-ikr}\zeta = -i\omega\frac{E_P}{d}C_{\text{ED}}\frac{\tilde{e}_{\text{in}}}{2\pi rc}e^{-ikr}\zeta. \quad (82)$$

Taking into account that $\tilde{I}_{\text{in}} \approx i\omega C_{\text{ED}}\tilde{e}_{\text{in}}$, leads to

$$\tilde{p}(r,0)|_{b=a} \approx -\zeta\frac{E_P}{d}\cdot\frac{\tilde{I}_{\text{in}}}{c}\cdot\frac{e^{-ikr}}{2\pi r}, \quad (83)$$

which, in the case of $\zeta=1$, is Walker's equation.[21] A better approximation is given by

$$\zeta \approx 2\rho c/(R_S+2\rho c), \quad (84)$$

which leads to what could be termed the "modified Walker's equation." The on-axis pressure response with damping is shown in Fig. 9, together with the efficiency and peak displacement at $w=0$. Figure 10 shows a comparison of the on-axis responses with and without damping (the level is reduced in order to accommodate the large undamped excursions), together with the high frequency approximation, where the SPL is given by: $\text{SPL}=20\log_{10}|\tilde{p}(r,0)/(20\times10^{-6})|$. The normalized directivity function $20\log_{10}|D(\theta)|/|D(0)|$ is plotted in Fig. 11 for various values of ka.

III. MEMBRANE IN AN INFINITE BAFFLE

A. Boundary conditions

The membrane shown in Fig. 1 is now mounted in an infinite baffle in the xy plane with its center at the origin and the uniform driving force $\tilde{p}_I$ is applied in the z direction. The membrane deflection $\tilde{\eta}(w)$ is then to be used as a parameter to couple it to the surrounding loss-free acoustic medium.

The monopole source elements and their images together form the membrane source. Since they are coincident in the plane of the infinite baffle, they combine to form elements of double strength. Hence our membrane may be modeled as a "breathing" membrane in free space. Due to the symmetry of the pressure fields on either side of the plane of symmetry, we have the following Neumann boundary condition on the front and rear surfaces of the infinite baffle:

$$\frac{\partial}{\partial z}\tilde{p}(w,z)|_{z=0\pm} = 0, \quad a < w \leqslant \infty. \quad (85)$$

Also, on the front and rear outer surfaces of the membrane, there is the coupling condition

$$\frac{\partial}{\partial z}\tilde{p}(w,z)|_{z=0\pm} = -ik\rho c\tilde{u}_0(w), \quad = k^2\rho c^2\eta(w) \quad 0 \leqslant w \leqslant a. \quad (86)$$

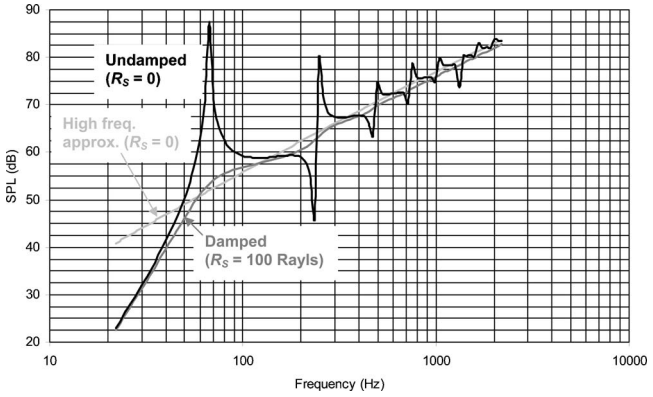

FIG. 10. On-axis pressure response with the same parameters as in Fig. 9, except $e_{\text{in}}=40$ V$_{\text{rms}}$, and with $R_S=0$ (undamped).

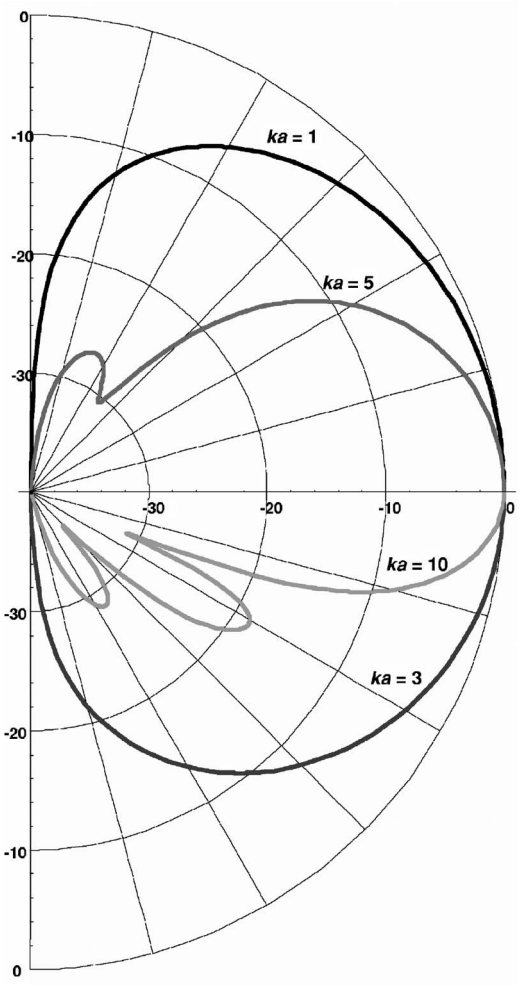

FIG. 11. Normalized far-field directivity function in free space with same parameters as in Fig. 9.

In the actual physical system (as opposed to the "breathing membrane" model), the pressure field on one side of the xy plane is the symmetrical "negative" of that on the other, so that

$$\tilde{p}(w,z) = -\tilde{p}(w,-z). \tag{87}$$

Again, the perimeter of the membrane is fixed, which leads to the boundary condition of Eq. (5). On the surface of the membrane, the velocity distribution $\tilde{u}_0(w_0)$ is defined, according to Bouwkamp's solution[6] to the free space wave equation in oblate spheroidal coordinates, as

$$\tilde{u}_0(w_0) = \sum_{m=0}^{\infty} \tilde{A}_m \left(1 - \frac{w_0^2}{a^2}\right)^{m+(1/2)}, \tag{88}$$

where $\tilde{A}_m$ are the as yet unknown power series coefficients.

B. Solution to the free space wave equation

Using the King integral and taking into account the double layer source, the pressure distribution is defined by

$$\tilde{p}(w,z) = 2\int_0^{2\pi}\int_0^a g(w,z|w_0,z_0) \times \frac{\partial}{\partial z_0}\tilde{p}\,(w_0,z_0)|_{z_0=0+} w_0 dw_0 d\phi_0, \tag{89}$$

where the Green's function[14] is defined, in axisymmetric cylindrical coordinates, by

$$g(w,z|w_0,z_0) = \frac{i}{4\pi}\int_0^{\infty} J_0(\mu w)J_0(\mu w_0)\frac{\mu}{\sigma}e^{-i\sigma|z-z_0|}d\mu, \tag{90}$$

where σ is defined by Eq. (8). Substituting Eqs. (86), (88), and (90) in Eq. (89) and integrating over the surface of the membrane yields

$$\tilde{p}(w,z) = ka\rho c\sum_{m=0}^{\infty}\tilde{A}_m\Gamma\left(m+\frac{3}{2}\right)\int_0^{\infty}\left(\frac{2}{a\mu}\right)^{m+(1/2)} \times J_0(w\mu)J_{m+(3/2)}(a\mu)\frac{e^{-i\sigma z}}{\sigma}d\mu, \tag{91}$$

where Sonine's integral of Eq. (26) has been used (with $\mu = \alpha_{0n}/a$). Setting $z=0$ yields the surface pressure as follows:

$$\tilde{p}_+(w_0) = ka\rho c\sum_{m=0}^{\infty}\tilde{A}_m\Gamma\left(m+\frac{3}{2}\right)\int_0^{\infty}\left(\frac{2}{a\mu}\right)^{m+(1/2)} \times J_0(w_0\mu)J_{m+(3/2)}(a\mu)\frac{1}{\sigma}d\mu. \tag{92}$$

C. Formulation of the coupled problem

Let the power series coefficients $\tilde{A}_m$ be related to normalized dimensionless coefficients τ_m by

$$\tilde{A}_m = \frac{\tau_m(m+3/2)}{2\rho c}\tilde{p}_I. \tag{93}$$

Substituting this together with Eq. (92) in Eq. (37) and integrating over ϕ_0 leads to the following coupled equation:

$$\tilde{\eta}(w) = \frac{2\pi}{T}\tilde{p}_I\int_0^a\left(\sum_{m=0}^{\infty}\tau_m I_m(w_0,k)-1\right)G(w|w_0)w_0dw_0. \tag{94}$$

The infinite integral I_m is defined by

$$I_m(w_0,k) = ka\Gamma\left(m+\frac{5}{2}\right)\int_0^{\infty}\left(\frac{2}{a\mu}\right)^{m+(1/2)} \times J_0(w_0\mu)J_{m+(3/2)}(a\mu)\frac{1}{\sigma}d\mu = I_{mR}(w_0,k)+iI_{mI}(w_0,k), \tag{95}$$

where the solution[10] to the real part is given by

$$I_{mR}(w_0,k) = \sqrt{\pi}\sum_{q=0}^{\infty}\sum_{r=0}^{\infty}\frac{(-1)^{q+r}\Gamma(m+5/2)\Gamma(q+r+1)}{(q!)^2 r!\Gamma(r+m+5/2)\Gamma(q+r+3/2)} \times\left(\frac{ka}{2}\right)^{2(q+r+1)}\left(\frac{w_0}{a}\right)^{2q}. \quad (96)$$

and the solution[10] to the imaginary part is given by

$$I_{mI}(w_0,k) = \sqrt{\pi}\sum_{q=0}^{\infty}\sum_{r=0}^{\infty}\frac{(-1)^{q+r+m+1}\Gamma(m+5/2)\Gamma(q+r-m-1/2)}{(q!)^2 r!\Gamma(r-m-1/2)\Gamma(q+r-m)} \times\left(\frac{ka}{2}\right)^{2(q+r-m)-1}\left(\frac{w_0}{a}\right)^{2q}. \quad (97)$$

For large ka, an approximation[16] is given by

$$I_m(w_0,k) \approx (m+3/2)\left(1-\frac{w_0^2}{a^2}\right)^{m+(1/2)}. \quad (98)$$

D. Bessel series expansion of the membrane deflection

Using the power series of Eq. (88) together with Eq. (93), the deflection can also be expressed as

$$\tilde{\eta}(w) = \frac{\tilde{u}_0(w)}{i\omega} = \frac{\tilde{p}_I}{2ik\rho c^2}\sum_{m=0}^{\infty}\tau_m\left(m+\frac{3}{2}\right)\left(1-\frac{w^2}{a^2}\right)^{m+(1/2)},$$

$$0 \leqslant w \leqslant a. \quad (99)$$

Using the Bessel series expansion from Eqs. (24) and (25), Eq. (99) can be written

$$\tilde{\eta}(w) = \frac{\tilde{p}_I}{2ik\rho c^2}\sum_{m=0}^{\infty}\tau_m\Gamma\left(m+\frac{5}{2}\right)\sum_{n=1}^{\infty}\left(\frac{2}{\alpha_n}\right)^{m+(3/2)} \times\frac{J_{m+(3/2)}(\alpha_n)}{J_1^2(\alpha_n)}\times J_0(\alpha_n w/a), \quad 0 \leqslant w \leqslant a. \quad (100)$$

E. Final set of simultaneous equations for the power series coefficients

1. Rigorous solution

Inserting Eq. (38) in Eq. (94), equating the right-hand sides of Eqs. (94) and (100), while integrating over the surface of the membrane using the identities of Eqs. (18) and (40) and then equating the coefficients of $J_0(\alpha_n w/a)$ yields the following set of $M+1$ simultaneous equations in τ_m;

$$\sum_{m=0}^{M}{}_m\Psi_n(k_D'a,ka)\tau_m = 1, \quad n = 1,2,\ldots,M+1, \quad (101)$$

where

$${}_m\Psi_n(k_D'a,ka) = \frac{\alpha_n}{2J_1(\alpha_n)}\left\{-ika\Gamma\left(m+\frac{5}{2}\right)\left(\frac{2}{\alpha_n}\right)^{m+(3/2)} \times J_{m+(3/2)}(\alpha_n)\frac{\alpha_n^2-k_D'^2a^2}{\alpha^2(ka)} + \sum_{q=0}^{Q}({}_{m+1}\mathbf{P}_q(ka)+i_{m+1}\mathbf{T}_q(ka)) \times\frac{{}_1F_2(q+1;1,q+2;-\alpha_n^2/4)}{q+1}\right\}, \quad (102)$$

where $\mathbf{P}$ and $\mathbf{T}$ are monopole cylindrical wave functions. $\mathbf{P}$ has been named the Spence function[10] as defined by

$${}_{m+1}\mathbf{P}_q(ka) = \sqrt{\pi}\sum_{r=0}^{R}\frac{(-1)^{q+r}(ka/2)^{2(q+r+1)}}{r!(q!)^2(m+5/2)_r(q+r+1)_{1/2}} \quad (103)$$

and $\mathbf{T}$ has been named the Stenzel function [10] as defined by

$${}_{m+1}\mathbf{T}_q(ka) = \sqrt{\pi}\sum_{r=0}^{R}\frac{(-1)^{q+r+m+1}(ka/2)^{2(q+r-m)-1}}{r!(q!)^2(m+5/2)_{r-2m-3}(q+r-m-1/2)_{1/2}}, \quad (104)$$

where the infinite series have been truncated to orders M, Q, and R. $\mathbf{P}$ and $\mathbf{T}$ are monopole cylindrical wave functions. The dimensionless parameter α is the fluid-loading factor, as defined by Eq. (43), and $(x)_n$ is the Pochhammer symbol. The calculations were performed using, in the case of the damped membrane, 50 digit precision with $M=10+ka$ and $Q=R=2M$. In the case of the undamped membrane, 100 digit precision was used with $M=10+5ka$ and again $Q=R=2M$.

2. High frequency approximation

For large values of ka, the following high-frequency approximation can be obtained by the same method as for the rigorous solution, except that Eq. (98) is used instead of Eq. (97) and the identity of Eq. (18) is replaced by Eq. (26) so that the solution is, not surprisingly, the same as that given in Eq. (44).

F. Impedance and efficiency

1. Input impedance

The total volume velocity $\tilde{U}_0$ produced by the membrane is equal to the integral of its velocity $\tilde{u}_0(w)$ $(=i\omega\tilde{\eta}(w))$ from Eq. (99) over its surface as follows:

$$\tilde{U}_0 = ikc\int_0^{2\pi}\int_0^a\tilde{\eta}(w)w\,dw\,d\phi = \frac{S\tilde{p}_I}{2\rho c}\sum_{m=0}^{\infty}\tau_m, \quad (105)$$

where $S=\pi a^2$ is the area of the membrane. The parameters z_{mi}, z_{E}, z_{ES}, and z_{EM} are given in Eqs. (47) and (49)–(51), respectively. The normalized motional input impedance Z_I is given by

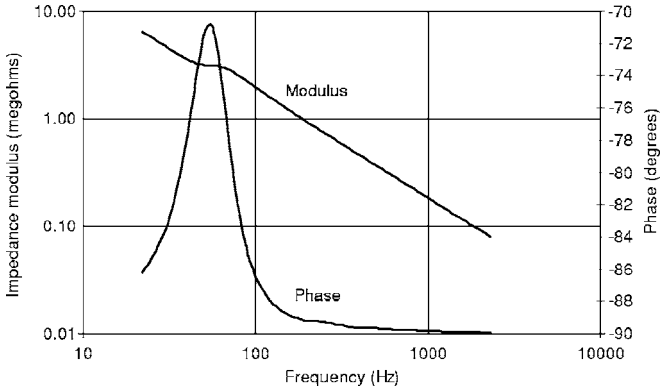

FIG. 12. Electrical input impedance of push-pull electrostatic loudspeaker in infinite baffle where $a=250$ mm, $h=12$ μm, $T=700$ N/m, $\rho_D=1400$ kg/m^3, $E_P=3000$ V, $d=2$ mm, $r=1$ m, and $R_S=100$ Ns/m^3.

$$Z_I = \frac{\tilde{F}_I}{2\rho c \tilde{U}_0} = \left(\sum_{m=0}^{M} \tau_m \right)^{-1}. \tag{106}$$

The input impedance for a damped membrane is shown in Fig. 12. Since the static impedance dominates, the motional impedance is plotted separately in Fig. 13.

2. Radiation impedance

The total radiation force $\tilde{F}_R$ acting upon the membrane can be found by integrating the surface pressure from Eq. (92) over its surface as

$$\begin{aligned} \tilde{F}_R &= -\int_0^{2\pi} \int_0^a \tilde{p}_+(w_0) w_0 dw_0 d\phi_0 \\ &= \frac{\tilde{F}_I}{2} ka \sum_{m=0}^{\infty} \tau_m \Gamma\left(m + \frac{5}{2}\right) \\ &\quad \times \int_0^{\infty} \left(\frac{2}{a\mu}\right)^{m+(3/2)} \frac{J_1(a\mu) J_{m+(3/2)}(a\mu)}{\sqrt{k^2 - \mu^2}} d\mu, \end{aligned} \tag{107}$$

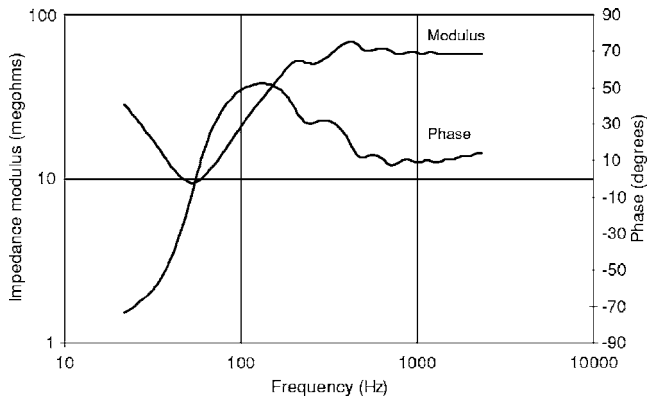

FIG. 13. Motional part of electrical impedance in infinite baffle with the same parameters as in Fig. 12.

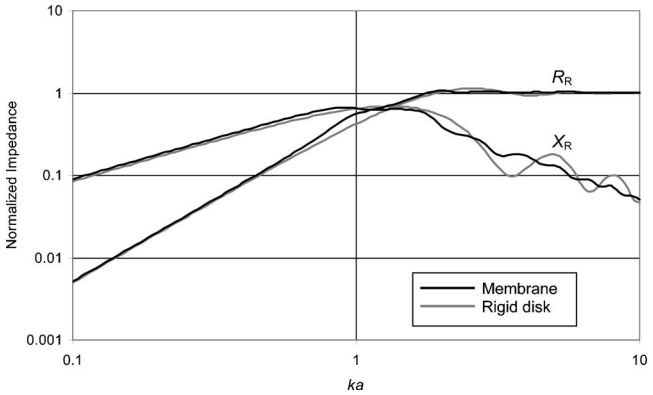

FIG. 14. Normalized radiation impedance in infinite baffle with the same parameters as in Fig. 12 and radiation impedance of a rigid disk in an infinite baffle.

where the identity of Eq. (40) has again been used. After solving the infinite integral,[15] the force transmission coefficient, defined in Eq. (53), is given by

$$\begin{aligned} \zeta = \sum_{m=0}^{M} \tau_m \Bigg\{ & 1 - {}_2F_3\left(\frac{m}{2} + \frac{3}{4}, \frac{m}{2} + \frac{5}{4}; \frac{1}{2}, m + \frac{3}{2}, m + \frac{5}{2}; -k^2a^2\right) \\ & + ika \frac{{}_2F_3\left(\frac{m}{2} + \frac{5}{4}, \frac{m}{2} + \frac{7}{4}; \frac{3}{2}, m + 2, m + 3; -k^2a^2\right)}{(m + 5/2)_{-1/2} (m + 5/2)_{1/2}} \Bigg\}. \end{aligned} \tag{108}$$

The acoustic radiation impedance z_{ar} is then given by Eq. (55), where R_R is the normalized radiation resistance given by $R_R = \Re(\zeta Z_I)$ and X_R is the normalized radiation *reactance* given by $X_R = \Im(\zeta Z_I)$. This result is plotted in Fig. 14 together with the radiation impedance of a rigid disk in an infinite baffle for comparison.

3. Efficiency

Now it is easy to calculate the efficiency which is simply equal to $100^* R_R/R_I$ and is shown in Fig. 17 along with the far-field on-axis pressure response and peak displacement.

4. Diaphragm impedance

The mechanical diaphragm impedance z_{md} is the difference between the input impedance and the radiation impedance on both sides, as defined by Eq. (56), where R_D is the normalized diaphragm *resistance* given by $R_D = \Re(Z_I(1-\zeta))$ and X_D is the normalized membrane *reactance* given by $X_D = \Im(Z_I(1-\zeta))$. This result is plotted in Fig. 15. The various impedances are shown on an equivalent electrical circuit in Fig. 7.

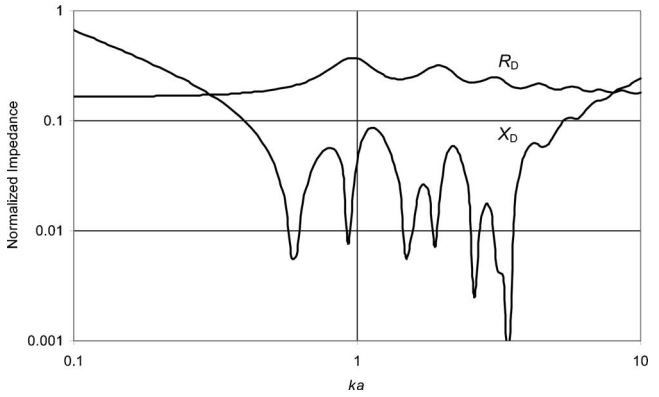

FIG. 15. Normalized diaphragm impedance in infinite baffle with the same parameters as in Fig. 12.

G. Near-field pressure response

1. Near-field pressure when the distance from the center of the membrane to the observation point is greater than the membrane's radius

Using the same procedure as in a recent paper for a resilient disk in an infinite baffle,[10] it can be shown that

$$p(r,\theta) = -\pi\tilde{p}_I \sum_{m=0}^{M}\sum_{p=0}^{P} \frac{\tau_m h_{2p}^{(2)}(kr) P_{2p}(\cos\theta)}{(m+(5/2))_p \Gamma((1/2)-p)\Gamma(2p+(1/2))} \times \left(\frac{ka}{2}\right)^{2p+2} {}_1F_2\left(p+1; p+m+\frac{5}{2}, 2p+\frac{3}{2}; -\frac{k^2a^2}{4}\right). \tag{109}$$

This solution converges providing $r \geqslant a$.

2. Near-field pressure when the distance from the center of the membrane to the observation point is less than the membrane's radius

a. Near-field pressure as an integral expression. After truncating the summation limit and inserting Eq. (93), Eq. (91) can be separated into finite and infinite integrals as follows:

$$\tilde{p}(w,z) = \tilde{p}_I \sum_{m=0}^{M} \tau_m \Gamma\left(m+\frac{5}{2}\right)(I_{\mathrm{Fin}}(m,w,z) - iI_{\mathrm{Inf}}(m,w,z)), \tag{110}$$

where

$$I_{\mathrm{Fin}}(m,w,z) = \frac{ka}{2}\int_0^k \left(\frac{2}{a\mu}\right)^{m+(1/2)} J_{m+(3/2)}(a\mu) \times J_0(w\mu)\frac{e^{-iz\sqrt{k^2-\mu^2}}}{\sqrt{k^2-\mu^2}}d\mu \tag{111}$$

and

$$I_{\mathrm{Inf}}(m,w,z) = \frac{ka}{2}\int_k^\infty \left(\frac{2}{a\mu}\right)^{m+(1/2)} J_{m+(3/2)}(a\mu) \times J_0(w\mu)\frac{e^{-z\sqrt{\mu^2-k^2}}}{\sqrt{\mu^2-k^2}}d\mu. \tag{112}$$

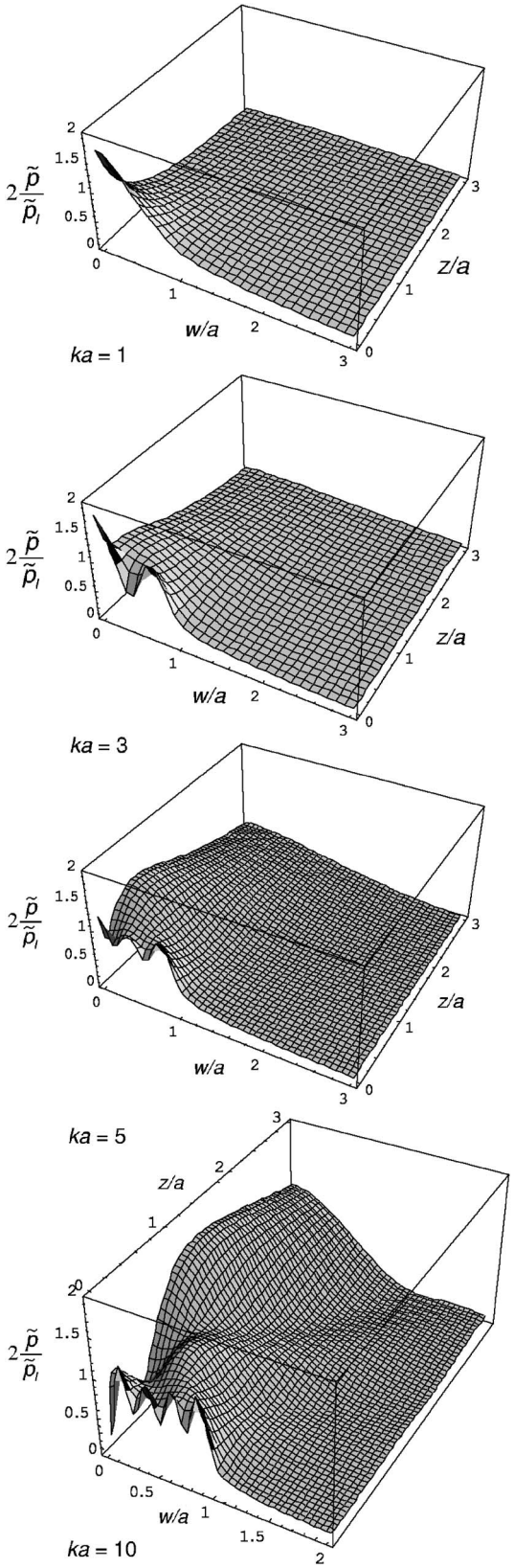

FIG. 16. Near-field pressure response in infinite baffle with the same parameters as in Fig. 12.

b. Solution of the finite integral. Using the same procedure as in a recent paper for a resilient disk in an infinite baffle,[10] it can be shown that

$$I_{\mathrm{Fin}}(m,w,z) = -\sum_{p=0}^{P}\sum_{q=0}^{Q}\frac{1}{p!q!(ikz)^{2(p+q)+1}}\left(\frac{ka}{2}\right)^{p-m+(1/2)} \times\left(\frac{kw}{2}\right)^{q} J_{p+m+(3/2)}(ka)J_q(kw) \times\gamma(2p+2q+1,ikz). \quad (113)$$

c. Solution of the infinite integral. Similarly, it can be shown that[10]

$$I_{\mathrm{Inf}}(m,w,z) = \left(\frac{2}{ka}\right)^{2m+1}\sum_{p=0}^{P}\sum_{q=0}^{Q}\frac{(-1)^{p+q}(2p+m+3/2)}{q!(k^2z^2+k^2a^2)^{q-(m/2)-(1/4)}} \times(p+1)_{m+(1/2)}\Gamma(2p+2q+1)\left(\frac{kw}{2}\right)^{q} \times J_{2p+m+(3/2)}(ka)J_q(kw)P^{-2p-m-(3/2)}_{2q-m-(3/2)} \times\left(\frac{z}{\sqrt{z^2+a^2}}\right). \quad (114)$$

The normalized near-field pressure response of the membrane is shown in Fig. 16 for various values of ka. The calculations were performed using 50 digit precision with $P=M=10+ka$ and $Q=2P$.

H. Far-field pressure response

The far-field pressure is derived using the same procedure as shown in Part I of Sec. II of a recent paper[10] to give the same result as Eq. (79), except that the directivity function $D(\theta)$ is now given by

$$D(\theta) = ka\sum_{m=0}^{M}\tau_m\Gamma\left(m+\frac{5}{2}\right)\left(\frac{2}{ka\sin\theta}\right)^{m+(3/2)} \times J_{m+(3/2)}(ka\sin\theta), \quad (115)$$

which is the same as for the free space membrane except for the absence of the cos θ term because the free space membrane is a dipole, whereas the baffled membrane is a monopole. For $\theta=0$ (i.e., on-axis), this simplifies to

$$D(0) = ka\sum_{m=0}^{M}\tau_m = \frac{ka}{Z_I}, \quad (116)$$

using Z_I from Eq. (106). Hence the on-axis pressure simplifies to

$$\tilde{p}(r,0) = i\frac{ka^2}{4r}\tilde{p}_I e^{-ikr}\frac{1}{Z_I} = i\omega\frac{E_P}{d}C_{\mathrm{ED}}\frac{\tilde{e}_{\mathrm{in}}}{2\pi rc}e^{-ikr}\frac{1}{Z_I}. \quad (117)$$

Taking into account that $\tilde{I}_{\mathrm{in}}\approx i\omega C_{\mathrm{ED}}\tilde{e}_{\mathrm{in}}$, leads to

$$\tilde{p}(r,0)|_{b=a} \approx \frac{1}{Z_I}\cdot\frac{E_P}{d}\cdot\frac{\tilde{I}_{\mathrm{in}}}{c}\cdot\frac{e^{-ikr}}{2\pi r}, \quad (118)$$

which, in the case of $Z_I=1$, is Walker's equation.[21] A better approximation is given by

$$Z_I \approx 1 + R_S/(2\rho c), \quad ka>2, \quad (119)$$

which leads to what could be termed the "modified Walker's equation." The on-axis pressure response with damping is shown in Fig. 17, together with the efficiency and peak displacement at $w=0$. In Fig. 18 is shown a comparison of the on-axis responses with and without damping (the level is reduced in order to accommodate the large undamped excursions), together with the high frequency approximation, where the SPL is given by: $\mathrm{SPL}=20\log_{10}|\tilde{p}(r,0)/(20\times10^{-6})|$. The normalized directivity function $20\log_{10}|D(\theta)|/|D(0)|$ is plotted in Fig. 19 for various values of ka.

IV. FINITE ELEMENT MODEL

Abaqus CAE v6.5-5 was used for the finite element analysis. In order to save processing power, only a quarter membrane was simulated. The analysis was carried out in two steps using a cylindrical coordinate system. In the first step, a boundary condition was applied to rim of the quarter membrane, which blocked axial or tangential displacement, but allowed radial displacement. Also, a boundary condition of zero tangential displacement was applied to its two straight edges. A pretension T was applied to the rim node set using the formula

$$\text{Force per node} = 0.5\pi aT/(\text{No. of nodes}). \quad (120)$$

The second step was a steady-state dynamics analysis in which an evenly distributed pressure of $\tilde{p}_{\mathrm{I}}=1$ Pa was applied to the membrane surface. A limitation is that there is no obvious way to simulate the viscous acoustic resistance presented by a perforated screen or mesh. The elements used for the simulation are described in Table I.

The membrane was surrounded by a quarter-sphere of air with a radius of 0.5 m. The outer curved surface of this quarter-sphere was coated with a skin of infinite elements in order to prevent reflections. The air space was created as two separate front and rear segments, which both had their adjoining faces partitioned where they met the rim of the membrane. Each was tied to one of the surfaces of the membrane and, in the case of the unbaffled membrane, to each other beyond the rim. Hence, in order to simulate an infinite baffle, the coupling between the air segments was omitted so that the rigid boundary condition at the baffle was created auto-

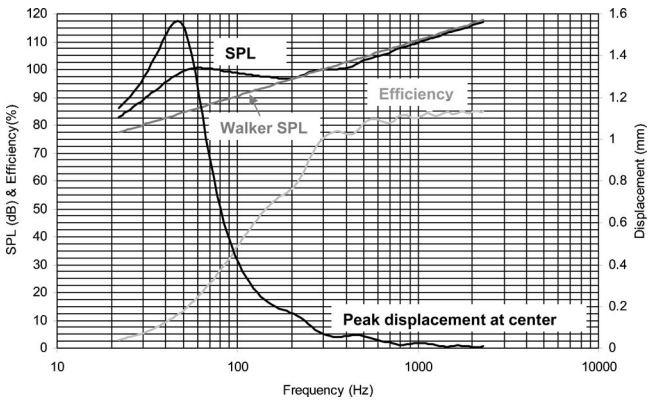

FIG. 17. On-axis pressure response of push-pull electrostatic loudspeaker in infinite baffle where $a=250$ mm, $h=12$ μm, T=700 N/m, $\rho_D=1400$ kg/m^3, $e_{\mathrm{in}}=2000$ V$_{\mathrm{rms}}$, $E_P=3000$ V, $d=2$ mm, $r=1$ m, and $R_S=100$ Ns/m^3.

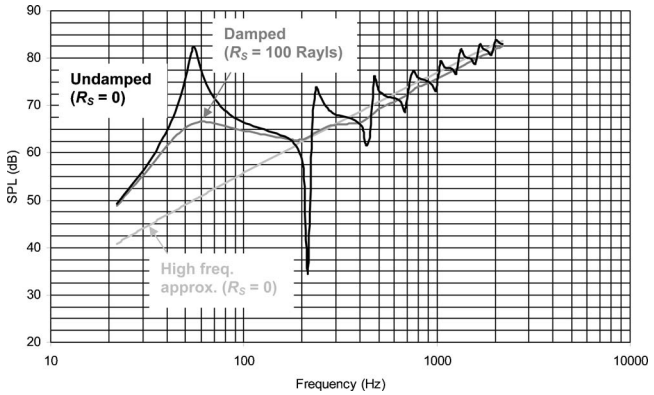

FIG. 18. On-axis pressure response with same parameters as in Fig. 18, except e_{in}=40 V_{rms}, and with R_S=0 (undamped).

matically without having to create a separate baffle surface. This also allowed the same mesh to be used for both simulations.

The outer curved edges of the air space were seeded with a node density of 80 nodes/m (or 6 nodes/wavelength in free space at 4.6 kHz). The edges of the membrane were seeded with higher density of 400 nodes/m (or 6 nodes/wavelength in the membrane at 4.7 kHz), as were also the adjacent edges of the air space to which its edges were tied. The remaining straight edges of the air space were left unseeded. Free meshing was used throughout. The total number of air elements was 588 757 with minimum and maximum angles of 7.5° and 143.4°, respectively. The number of membrane elements was 4824 with minimum and maximum angles of 29° and 115°, respectively. The finite size of the air space produced some errors below 170 Hz, so the analysis at these frequencies was performed using a 2.5 m radius quarter-sphere with a coarser mesh density to save memory and processing time. The on-axis responses without and with a baffle are shown in Figs. 20 and 21, respectively.

V. DISCUSSION

At low to medium frequencies, the analytical calculations and FEM results show excellent agreement, as can be seen in Figs. 20 and 21. However, above 1 kHz some divergence occurs. This is in no doubt partly due to the discretization of the finite element model, which has a density of 6 elements per wavelength at the highest frequency shown. There could also be some differences due to the fact that the FEM response was calculated at a distance 0.5 m from the source and then adjusted to 1 m by subtracting 6 dB, whereas the analytical result was calculated using the far-field asymptotic expression. The analytical calculations for the free space membrane without damping show good agreement with Streng's results[5] too.

It is interesting to see how the free space radiation impedance in Fig. 5 is an almost monotonic function when compared with that of a rigid disc. In this respect, it is more like that of a resilient disc in free space [13] (or "freely suspended disc"),[14] which is perhaps not surprising, considering that the membrane is essentially a more or less evenly distributed pressure source (i.e., transparent) rather than velocity one (or opaque). As can be seen from the near-field pressure plots of Fig. 8, the surface pressure becomes more evenly distributed at higher values of *ka*. However, one important difference between a membrane and a resilient disc is that the membrane is clamped at its outer edge whereas the resilient disc is free and therefore not realizable.[13] Interestingly, the real part of the membrane's radiation impedance at low frequencies is greater than that of the rigid disk, possibly due to the fact that its perimeter is clamped so that most of the sound is radiated from the center, with the remainder acting as a semibaffle to mitigate the acoustic "short-circuit" between the front and rear surfaces.

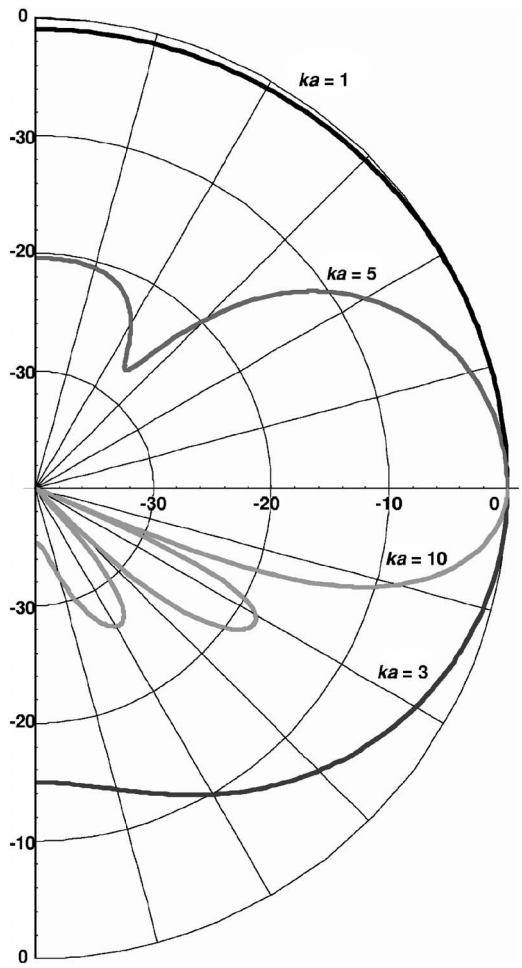

FIG. 19. Normalized far-field directivity function in infinite baffle with same parameters as in Fig. 17.

The baffled radiation impedance in Fig. 14 is also a fairly smooth function, compared to that of a rigid disk, and is therefore closer to the characteristic of a resilient disk in an infinite baffle[10] (or plane wave diffracted through a circu-

TABLE I. Summary of the finite element model.

Material	Section type	Element type
Membrane	Membrane	M3D3 Tri, 3 Node Triangular Membrane
Air	Solid Homogeneous	AC3D4 Tet, 4 Node Linear Acoustic Tetrahedron
Air	Solid Homogeneous.	ACIN3D3 Tri, 3 Node Acoustic Infinite

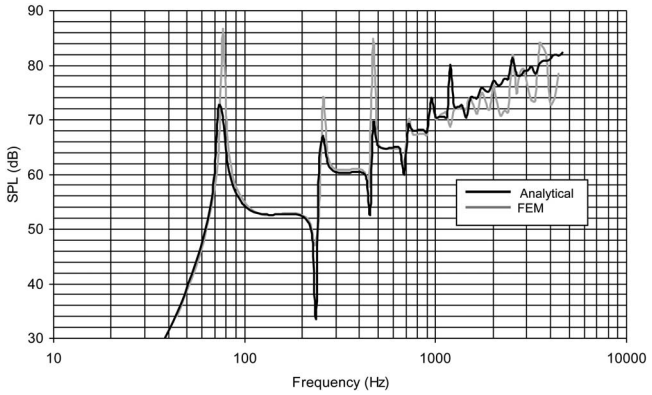

FIG. 20. On-axis pressure response in free space without damping: comparison of analytical and FEM models, where $a=125$ mm, $h=12$ μm, $T=100$ N/m, $\rho_D=1667$ kg/m^3, $p_I=1$ Pa, $r=1$ m, and $z_S=0$.

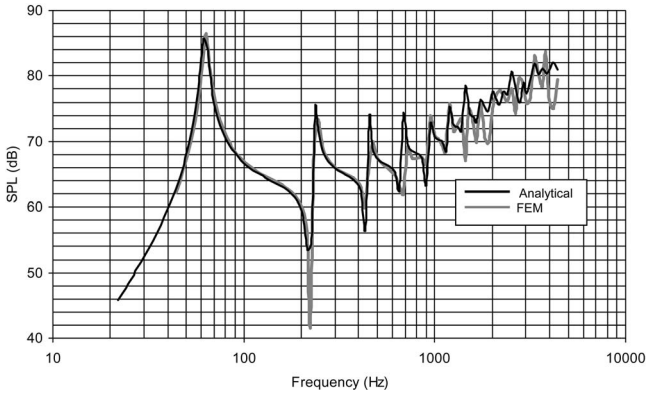

FIG. 21. On-axis pressure response in infinite baffle without damping: comparison of analytical and FEM models, where $a=125$ mm, $h=12$ μm, $T=100$ N/m, $\rho_D=1667$ kg/m^3, $p_I=1$ Pa, $r=1$ m, and $z_S=0$.

lar aperture)[6]. As can be seen from the near-field pressure plots of Fig. 16, the surface pressure eventually becomes more evenly distributed at higher values of ka and so converges towards the flat pressure distribution of a resilient disk.

It can be seen from Figs. 4 and 13 that the motional impedance in the "piston range" above 440 Hz (or $ka>2$) is mainly resistive, as is also the radiation impedance shown in Figs. 5 and 14. In this region, as the commonly used term "piston range" suggests, the diaphragm effectively radiates sound power into the surrounding space and it is here that the efficiency (see Figs. 9 and 17) is highest. The rising on-axis response in this region appears to be fairly consistent with that predicted by Walker's equation, a fairly detailed discussion of which is provided by Baxendall[1] (edited by Borwick). This equation generally describes the free space on-axis pressure response (with some damping) between the fundamental resonance and the point at which the diaphragm inertia, together with the acoustic (mainly radiation) resistance, starts to take control. If the electrode structure were to be partitioned into concentric rings, as described by Walker,[21] the on-axis response in the piston range could, in theory, be equalized and it would be interesting to see this included in the model. Also, the polar responses of Figs. 11 and 19 could be widened without losing power. The effect of the baffle is to equalize the on-axis response in the lower frequency range ($ka>2$) so that, with electrode partitioning, it could be fairly flat all the way from the fundamental resonance to the high frequency roll-off, at which the diaphragm inertia begins to dominate.

The motional impedance has a minimum value at the fundamental resonance, which is at 67 Hz in free space (see Fig. 4) and 53 Hz in a baffle (see Fig. 13). Here, the efficiency is lowest because most of the power is being dissipated in the acoustic damping resistance. (This behavior is in contrast with that of an electrodynamic loudspeaker, which tends to be most efficient at the suspension resonance and then becomes less efficient with increasing frequency.) Not surprisingly, adding a baffle greatly improves the efficiency in this region. Below the fundamental resonance, the slope of the on-axis response is 18 dB/octave in free space and 12 dB/octave in a baffle.

VI. CONCLUSIONS

A more direct method has been presented for calculating the radiation characteristics of a circular membrane in free space than previously available. Furthermore, the method has been extended to allow for the inclusion of an infinite baffle. In particular, equations have been derived for the motional impedance and diaphragm impedance, as well as expansions for the pressure field. The final equations for calculating the power series coefficients of the free space and baffled membranes are remarkably similar in form. Most of the terms are the same, but are just arranged differently. However, the pressure field is much easier to calculate for the baffled membrane when the distance to the observation point is greater than its radius.

It has also been shown how this model can be used as a benchmark for simulation using tools such as FEM. It is not intended, though, in this analytical versus FEM comparison, to select a "winner." On the contrary, the two approaches appear to be somewhat complementary. Whereas FEM is better suited to complicated geometries, analytical simulations tend to be limited to simply geometry, typically axisymmetric (i.e., two-dimensional). On the other hand, the analytical approach has distinct advantages at the frequency extremes and in deriving far-field asymptotic expressions. Furthermore, describing a model with equations provides us with a greater insight into the actual physics of the problem.

ACKNOWLEDGMENTS

The authors would like to express their gratitude to N. Lobo for his advice in numerical matters and are indebted to J. H. Streng for his invaluable discussions.

[1] J. Borwick, *Loudspeaker and Headphone Handbook*, 3rd ed. (Focal, Oxford, 2001), pp. 108–195.
[2] J. Zemanek, "Beam behaviour within the nearfield of a vibrating piston," J. Acoust. Soc. Am. **49**(1), 181–191 (1971).
[3] A. Nisbett, *The Use of Microphones*, 4th ed. (Focal, Oxford, 1993), p. 44.
[4] J. H. Streng, "Calculation of the surface pressure on a vibrating circular stretched membrane in free space," J. Acoust. Soc. Am. **82**(2), 679–686 (1987).

[5]J. H. Streng, "Sound radiation from a circular stretched membrane in free space," J. Audio Eng. Soc. **37**(3), 107–118 (1989).
[6]C. J. Bouwkamp, "Theoretical and numerical treatment of diffraction through a circular aperture," Indian J. Pure Appl. Phys. **AP18**(2), 152–176 (1970).
[7]P. M. Morse and K. U. Ingard, *Theoretical Acoustics* (McGraw-Hill, New York, 1968), pp. 320, 365, 389, 390.
[8]R. D. Spence, "The diffraction of sound by circular disks and apertures," J. Acoust. Soc. Am. **20**(4), 380–386 (1948).
[9]R. D. Spence, "A note on the Kirchhoff approximation in diffraction theory," J. Acoust. Soc. Am. **21**(2), 98–100 (1949).
[10]T. J. Mellow, "On the sound field of a resilient disk in an infinite baffle," J. Acoust. Soc. Am. **120**(1), 90–101 (2006).
[11]H. Suzuki and J. Tichy, "Sound radiation from an elastically supported circular plate," J. Acoust. Soc. Am. **65**(1), 106–111 (1979).
[12]T. J. Mellow and L. M. Kärkkäinen, "On the sound field of a membrane in an infinite baffle," on the CD ROM: Audio Engineering Society Convention Papers, 118th Convention, Barcelona, 28–31 May 2005, available from Audio Engineering Society Inc., 60 East 42nd Street, Room 2520, New York, NY 10165–2520.
[13]T. J. Mellow and L. M. Kärkkäinen, "On the sound field of an oscillating disk in an open and closed circular baffle," J. Acoust. Soc. Am. **118**(3), 1311–1325 (2005).
[14]I. S. Gradshteyn and I. M. Ryzhik, *Table of Integrals, Series, and Products*, 6th ed., edited by A. Jeffrey (Academic, New York, 2000), p. 658, Eq. (6.521.1), p. 671, Eq. (6.567.1), p. 668, Eq. (6.561.5), p. 342, Eq. (3.381.1), p. 930, Eq. (8.532.1), p. 980, Eq. (8.930.1)–(8.930.7), p. 342, Eq. (3.381.4), p. 891, Eq. (8.356.3), p. 691, Eq. (6.621.1).
[15]S. Wolfram, *The Mathematica Book*, 5th ed. (Wolfram Media, Champaign, IL, 2003). Symbolic computation by MATHEMATICA.
[16]M. Abramowitz and I. A. Stegun, *Handbook of Mathematical Functions* (Dover, New York, 1964), pp. 487, Eq. (11.4.41).
[17]L. L. Beranek, *Acoustics* (Acoustical Society of America, New York, 1993), pp. 101–105, 118–128.
[18]M. R. Stinson, "The propagation of plane sound waves in narrow and wide circular tubes, and generalization to uniform tubes of arbitrary cross-sectional shape," J. Acoust. Soc. Am. **89**(2), 1311–1325 (2005).
[19]G. N. Watson, *A Treatise on the Theory of Bessel Functions*, 2nd ed. (Cambridge University Press, London, 1944), pp. 141, Sec. 5.22, Eq. (5).
[20]A. O. Williams, "Acoustic field of a circular plane piston," J. Acoust. Soc. Am. **36**(12), 2408–2410 (1964).
[21]P. J. Walker, "New Developments in Electrostatic Loudspeakers," J. Audio Eng. Soc. **28**(11), 795–799 (1980).